PROCEEDINGS OF SPIE

SPIEDigitalLibrary.org/conference-proceedings-of-spie

Filters design and characterization for LAD instrument onboard eXTP

Ugo Lo Cicero, Marco Barbera, Nicola Montinaro, Fabio D'Anca, Michela Todaro, et al.

Ugo Lo Cicero, Marco Barbera, Nicola Montinaro, Fabio D'Anca, Michela Todaro, Elena Puccio, Luisa Sciortino, Filippo Ambrosino, Riccardo Campana, Tianxiang Chen, Yong Chen, Yuri Evangelista, Marco Feroci, Na Gao, Fangjun Lu, Yupeng Xu, Levent Cibik, Michael Krumrey, "Filters design and characterization for LAD instrument onboard eXTP," Proc. SPIE 12181, Space Telescopes and Instrumentation 2022: Ultraviolet to Gamma Ray, 121816H (31 August 2022); doi: 10.1117/12.2631556

SPIE.

Event: SPIE Astronomical Telescopes + Instrumentation, 2022, Montréal, Québec, Canada

Filters design and characterization for LAD instrument onboard eXTP

Ugo Lo Cicero[a,b], Marco Barbera[b,a], Nicola Montinaro[c,a], Fabio D'Anca[a,b], Michela Todaro[b,a], Elena Puccio[b,a], Luisa Sciortino[b,a], Filippo Ambrosino[d], Riccardo Campana[e], Tianxiang Chen[f], Yong Chen[f], Yuri Evangelista[d,g], Marco Feroci[d,g], Na Gao[f], Fangjun Lu[f], Yupeng Xu[f], Levent Cibik[h], and Michael Krumrey[h]

[a]Istituto Nazionale di Astrofisica – Osservatorio Astronomico di Palermo, Italy
[b]Università degli Studi di Palermo – Dipartimento di Fisica e Chimica, Italy
[c]Université de Genève, Département d'Astronomie, Switzerland
[d]Istituto Nazionale di Astrofisica – Istituto di Astrofisica e Planetologia Spaziali, Italy
[e]Istituto Nazionale di Astrofisica - Osservatorio di Astrofisica e Scienza dello Spazio, Italy
[f]Institute of High Energy Physics, China
[g]Istituto Nazionale di Fisica Nucleare – Sezione Tor Vergata, Italy
[h]Physikalisch-Technische Bundesanstalt (PTB), Germany

ABSTRACT

The LAD (Large Area Detector) instrument, onboard the Sino-European mission eXTP (enhanced X-ray Timing and Polarimetry), will perform single-photon, high-resolution timing and energy measurements, in the energy range 2–30 keV, with a large collecting area. Its silicon drift detectors need shielding from NIR/Vis/UV light by astrophysical sources and the bright Earth, to avoid performance degradation. Filters made of an Al coated thin polyimide (PI) membrane will guarantee the needed out-of-band rejection while offering high X-ray transparency. They will be placed between the detectors and the capillary plate plate collimators, open to the external environment. The mission is now in phase B2 and a baseline design for the filters was produced. We describe the filter design and modeling activity, and report the characterization performed so far on X-ray transmission, pinhole and defects, thermo-vacuum cycling endurance, and bright Earth optical load shielding properties.

Keywords: exTP, LAD, X-ray, filters, thin membrane

1. INTRODUCTION

eXTP (enhanced X-ray Timing and Polarimetry)[1] is an X-ray astronomy Sino-European mission currently in its phase B2. It is a "flagship" mission of the Chinese Academy of Science (CAS) and China National Space Administration (CNSA) that aims to study matter and physics in extreme conditions in terms of density and gravity and in presence of extreme magnetic fields. The payload development is led in China by IHEP/CAS and in Europe by INAF (Italy) and ICE-CSIC (Spain), and consists of four instruments: Large Area Detector (LAD), Wide Field Monitor (WFM), Spectroscopy Focusing Array (SFA), and Polarimetry Focusing Array (PFA). The European consortium includes institutes in Italy, Spain, Germany, France, Switzerland, Denmark, UK, Czech Republic, Poland.

The LAD instrument[2] will perform single-photon, high-resolution timing and energy measurements, in the energy range 2–30 keV, over a very large collecting area. Its Silicon Drift Detectors have to be shielded by IR/Vis/UV light, especially from the bright Earth emission, to avoid performance degradation. Thin filters will supply the needed out-of-band radiation rejection while providing high X-ray transparency in the energy range of interest. They will be placed between the detectors and the instrument capillary plate collimators, open to the external environment. This work focuses on the design of the filters and some characterization test to which they

Contact author: U. Lo Cicero
E-mail: ugo.locicero@inaf.it

Space Telescopes and Instrumentation 2022: Ultraviolet to Gamma Ray, edited by Jan-Willem A. den Herder, Shouleh Nikzad, Kazuhiro Nakazawa, Proc. of SPIE Vol. 12181, 121816H · © 2022 SPIE · 0277-786X · doi: 10.1117/12.2631556

are subject, while a previous work[3] focused on the manufacturing technology, heritage of the HXMT mission.[4] The first section reports the filter design choices and the modeling used to support them; the second section shows the simulated performances of the filters; the third section reports a set of characterization tests performed on filter samples.

2. FILTERS DESIGN

2.1 Filter requirements

The silicon drift detectors (SDD) at the heart of the LAD are very sensitive to the light. They need to be operated in a dark environment, since a very small amount of light in the spectral range between the IR to the UV would generate a current adding up to the signals generated by X-rays photons. To avoid performance degradation, the filters are required to provide an attenuation $> 10^8$ for all wavelengths in the range 10^2–10^3 nm. On the other hand, for the instrument to meet the effective area requirement, the filters transparency at 2.5 keV needs to be > 0.85 (as high as possible). The filters need as well to be able to withstand the launch vibrations and limited amount of differential pressure due to unbalanced air evacuation during launch. Once in the planned low Earth orbit they will have to resist to the aggressive action of highly reactive atomic oxygen, with an estimated fluence of about $2.3 \cdot 10^{22}$ atoms/cm^2 over the 5-years lifetime of the mission.

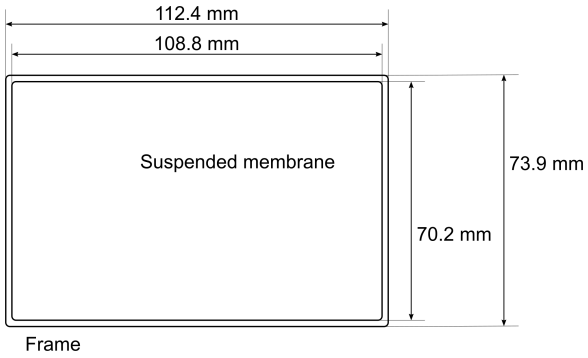

Figure 1. Schematic drawing of a LAD filter, showing the thin membrane suspended over an external frame

2.2 Filter design

The current filter design is based on the heritage from past missions such as Chandra,[5] from development activities performed for the LOFT mission study[6] and from knowledge gained with the study and activities performed for future X-ray missions such as Athena.[7,8] Each filter consists of a thin membrane suspended on a supporting frame. The material of choice for the frame is currently under selection; a 400 μm silicon frame can be directly manufactured during the membrane production process, but the use of metal frames is been considered as well. The material selected for the membrane is polyimide (PI), coated with aluminum. This combination of materials has been successfully employed in several X-ray missions, including the aforementioned ones. A modeling of the filter transmission has been used to select a design able to obtain the performances shown in the next sections. The resulting baseline design consists in 2 μm of PI and 200 nm of Al. A single layer of aluminum has been selected as the baseline choice. A double aluminum layer, that is an Al-PI-Al sandwich, would strongly reduce the probability of having pinholes through all the aluminum thickness, since such pinholes are generated by the random presence of particles during the metal deposition, and it would be highly unlikely to have two matching pinholes on the two aluminum layers. On the other hand, while pinholes can be avoided improving the cleanliness of the production environment, the double layer of aluminum brings a drawback concerning the filter susceptibility to atomic oxygen. There is evidence[9] that a sandwich structure causes a trapping effect, which can significantly worsen the PI erosion due to oxygen atoms that happen to penetrate the Al barrier. A second reason for preferring a single Al layer is related to the quality of the coating: an Al deposition over a membrane still placed on the flat substrate where it is formed has a quality significantly superior to the deposition done on a free-standing membrane, after it is released from the substrate; the double-side Al coating implies a deposition

on the free-standing membrane, thus an aluminum layer with lower quality and consequent lower IR/Vis/UV attenuation performance.

2.3 Modeling

Modeling the optical properties of the filter membrane is a key step to the design process. To calculate the transmittance and reflectance of the multi-layer film we adopt a matrix method[10] based on the Fresnel equations that require the knowledge of the refractive index of the materials and their thickness. We include in the model the layers of natural oxide that grow onto the Al surfaces (both on the Al-air interface and the PI-Al one). The refractive index of the PI is calculated with the model reported in 11; for wavelengths shorter than the validity of the model the refractive index is computed from the atomic scattering factors tabulated by Henke.[12] For the aluminum and its oxide we use a patchwork of tabulated data from Palik,[13] Hagemann,[14] Rakić[15] and Henke.[12]

2.4 X-ray performance

The model described in the previous section has been employed to calculate the expected performance in terms of X-ray transmission. Fig. 2.4 shows that a 2 μm thick PI membrane can meet the transmittance requirements at 2.5 keV if coated with up to 300 nm of aluminum.

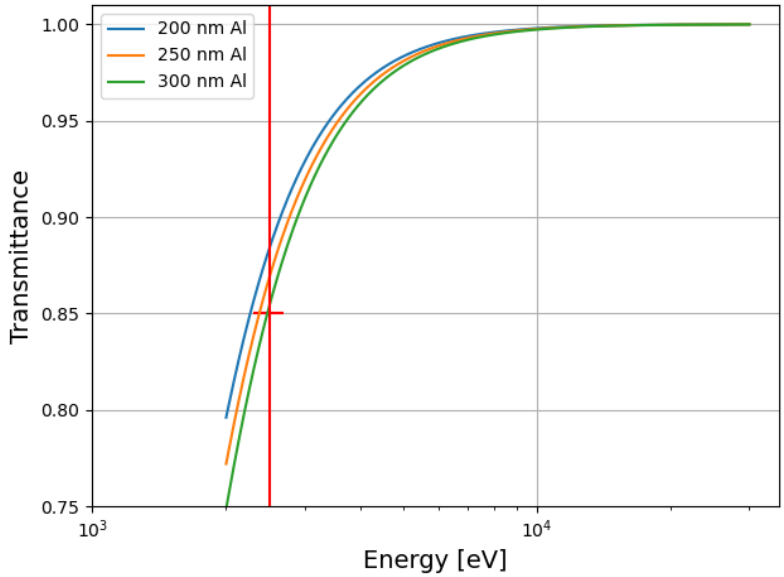

Figure 2. Modeled X-ray transmittance for a 2 μm thick PI membrane, with different thickness of aluminum coating. The red lines indicate the requirement at 2.5 keV.

2.5 IR/Vis/UV performance

The modeled transmission for the baseline filter in the IR/Vis/UV range is reported in Fig. 3. The transmittance in the full range is below 10^{-10}, with a very pronounced attenuation for wavelengths up to about 400 nm due to the presence of the PI. For higher wavelengths the main effect is the reflection provided by the aluminum. The modeled transmittance is used to calculate the effects of light from the Earth as shown in the next section.

2.6 Bright Earth effects

The most critical light source that can degrade the LAD performance is the Earth. It emits a considerable light flux and can appear within the field-of-view of the instrument. The spectrum contains two contributions, the flux coming from the Sun, 30.5% (worst seasonal case) of which is reflected by Earth,[16,17] and the thermal radiation emitted directly by the Earth. We model the first contribution with a black body emission from a Lambertian disk with Earth diameter (projected Earth) at the temperature of the Sun (5778 K), normalized for

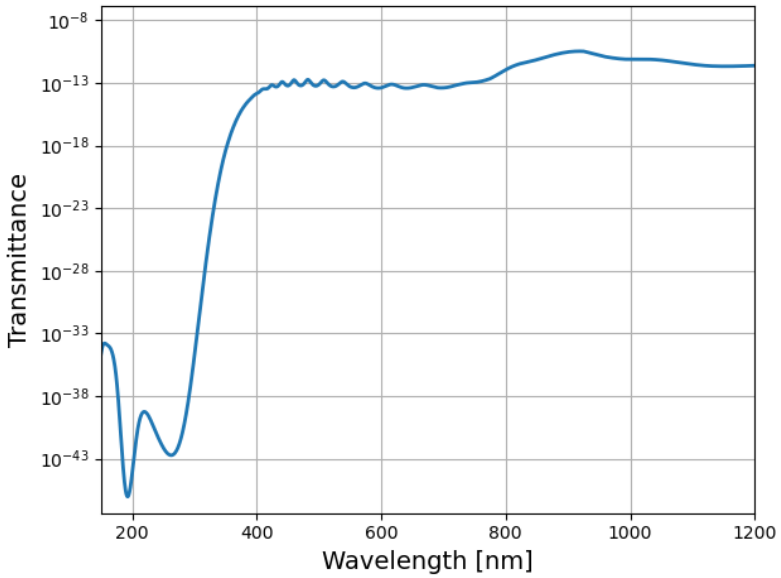

Figure 3. Modeled IR/Vis/UV transmittance for a 2 μm thick PI membrane, with 200 nm of aluminum coating.

a power density over the integrated spectrum of 417 W/m^2 (30.5% of the Sun power density outside the Earth atmosphere - 1366 W/m^2). The second contribution is modeled as emission from a black body at 288 K (average Earth surface temperature), normalized considering that it represents the reprocessed Sun power absorbed by the surface, which is about 950 W/m^2. Each detector, with an area of 42 mm^2, and situated at about 500 km above the Earth surface, subtends a solid angle of about $9{\cdot}10^{-13}$ sr. Fig. 4 shows the bright Earth unfiltered power spectral density at the detector, indicating the two contributions together with a gray line representing the Si gap, which is the upper limit of the detector sensitivity range. It is evident that the thermal emission from the Earth does not contribute to the detector noise, since it lays at wavelengths higher than the Si gap.

A trade-off study was performed calculating the number of electron-hole pairs produced into the detector, within its integration time (1 μs), by the filtered bright Earth radiation. As a worst case a 100% quantum efficiency was assumed for the detector throughout all the relevant spectrum. This study was performed by varying the thickness of the filter layers, with the requirement of having a maximum of 3 pairs, value that has been calculated to be generating a dark current that would not degrade the detector performance. Fig. 5 shows the number of electron-hole pairs generated using a filter with 2 μm PI vs. the deposited aluminum coating thickness. It can be seen that the number of pairs produced with the selected Al thickness, 200 nm, falls well below the 3 pairs threshold, thus meeting the requirement with a good margin. When more advanced prototypes will be characterized, thus allowing to reduce the margins, the X-ray transmission could be improved by further reducing the PI or the Al thickness, although it has to be taken in account that the aluminum is also needed to protect the PI from the atomic oxygen, and a too thin layer could easily present imperfections allowing the AO to pass trough.

3. EXPERIMENTAL CHARACTERIZATIONS

3.1 X-ray transmittance

High spectral-resolution transmission measurements were performed in two synchrotron facilities on a scaled filter prototype with baseline design, 2 um PI coated with 200 nm of Al. The main goals of these experimental campaigns were to verify the X-ray transmission compliance with the requirements, in particular at 2.5 keV, and to verify the thickness of the layers against the nominal values.

The X-ray transmission measurements were performed in two different external facilities: four-crystal monochromator (FCM) beamline[18] (in the photon energy range from 1.75 keV to 3.6 keV) in the PTB laboratory at the

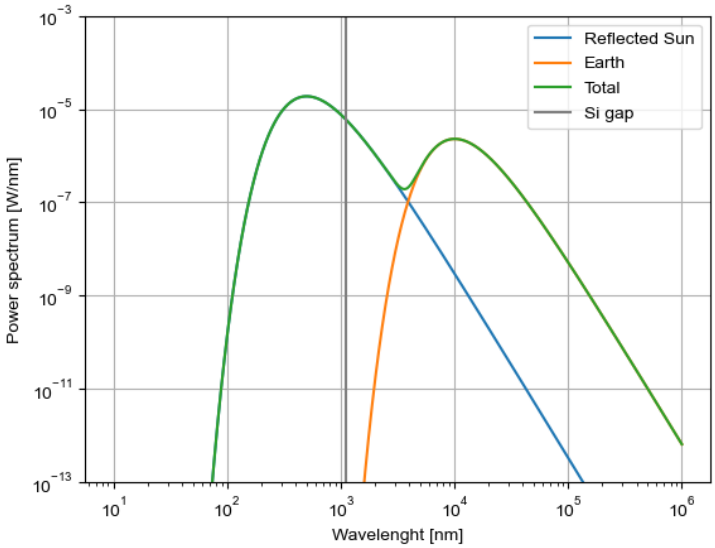

Figure 4. Modeled bright Earth unfiltered power spectral density at the detector. Blue line: reflected sunlight contribution; orange line: thermal emission from Earth; green line: sum of the two contributions; gray line: Si gap.

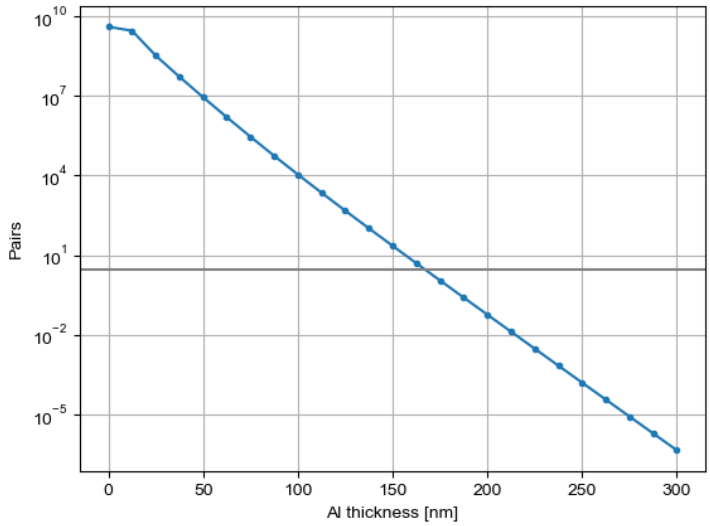

Figure 5. Calculation of electron-hole pairs produced by the filtered bright Earth spectrum within 1 μs integration time as a function of the Al coating thickness on a 2 μm thick PI filter. The gray line represents a value of 3 pairs.

BESSY II synchrotron radiation facility in Berlin, and BEAR beamline[19] (in the photon energy range from 50 eV to 1300 eV) at Elettra synchrotron in Trieste. The energy range investigated at BEAR includes edges of the elements present in the filter: Al L-edges (73 eV and 118 eV), C K-edge (282 eV), N K-edge (402 eV), and O K-edge (532 eV).

Fig. 6 reports the results of the measurements, showing that the transmission at 2.5 keV is 0.9, thus meeting the requirement (> 0.85). To estimate the thickness of the materials that make up the filter, the X-ray transmission data on the overall energy range 40–3600 eV was analyzed, by using the transmission model described in sec. 2.3 to fit the experimental data outside the edge regions. In Fig. 6, the X-ray transmission curve of the

sample is reported together with its best fitting curve. The relative deviation between experimental data and fit, reported in Fig. 7, is within ±10% for energies higher than 600 eV, whereas for lower energies, the accordance data-fit is worst as the filter is too opaque. In tab. 1, the estimation of the thicknesses of the materials of which the sample is made of are reported.

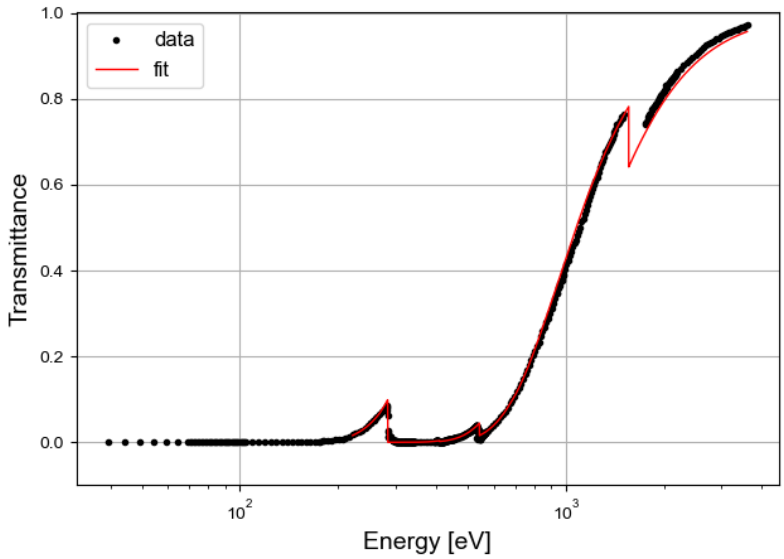

Figure 6. X-ray transmission data of nominal PI 2 um / Al 200 nm sample (black points) together with the fitting model (red line).

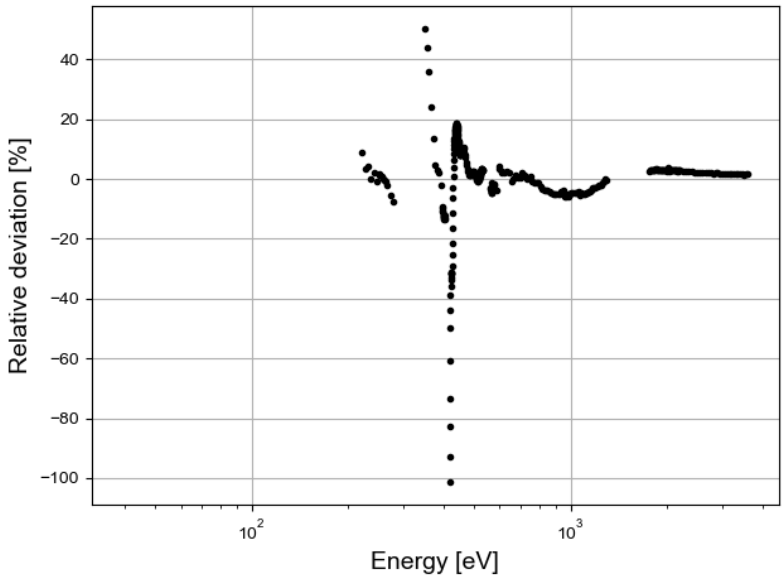

Figure 7. Relative deviation between data and fit as a function of the energy.

The thickness of PI membrane reported in tab. 1 is in good agreement with the nominal one, 6% higher. The aluminum thickness is 4% lower than the nominal value. It is worth noting that the aluminum oxide has been excluded from the model, because of the difficulty of assigning the Al atoms to the metal or to the oxide during the fit, causing 3σ variances for the two materials that amount to the same calculated value of the Al_2O_3

Table 1. Material nominal and measured thicknesses along with their 3σ variance.

Material	Nominal thickness [nm]	Measured thickness [nm]	3σ [nm]
Poly	2000	2112.4	9.9
Al	200	192.3	2.2

thickness. The oxide is expected to have a total thickness of about 7 nm distributed over two layers on the two sides of the aluminum.

Further synchrotron X-ray transmission measurements will be performed on the filters manufactured by the industry, complemented by X-ray imaging characterization to be performed at INAF-OAPA XACT facility[20] for measuring filter uniformity.

3.2 Pinholes

The presence of pinholes in the aluminum coating can severely affect the filter performance. A hole with a diameter of about 1 μm would let through a radiation flux equivalent to the flux transmitted by the whole filter, considering an attenuation of 10^{-10}. Moreover, an opening in the aluminum constitutes an entrance window for the atomic oxygen, that can significantly deteriorate the PI membrane. For these reasons, it is imperative to be able to detect pinholes in the filters; two systems at INAF-OAPA laboratories will be used to test the LAD filters for pinholes, an EPSON Perfection V850 Pro high-resolution scanner, and a Keyence VHX-7000 digital microscope. The scanner is used to quickly obtain transmission images of the filters to identify pinholes with a diameter > 10 μm, while the high magnification (up to 2500x) of the microscope, with its automation capabilities, allows to locate smaller pinholes.

The first prototypes were affected by severe pinhole presence, as visible in Fig. 8, but the issue was solved by IHEP with the implementation of stricter handling protocols and an increased cleanliness of the production environment (at time of writing there are no available images of the second generation prototypes acquired with the high resolution scanner). Filters produced by the industry are expected to have an even lower probability of a pinhole to occur thanks to the further enhanced environment cleanliness.

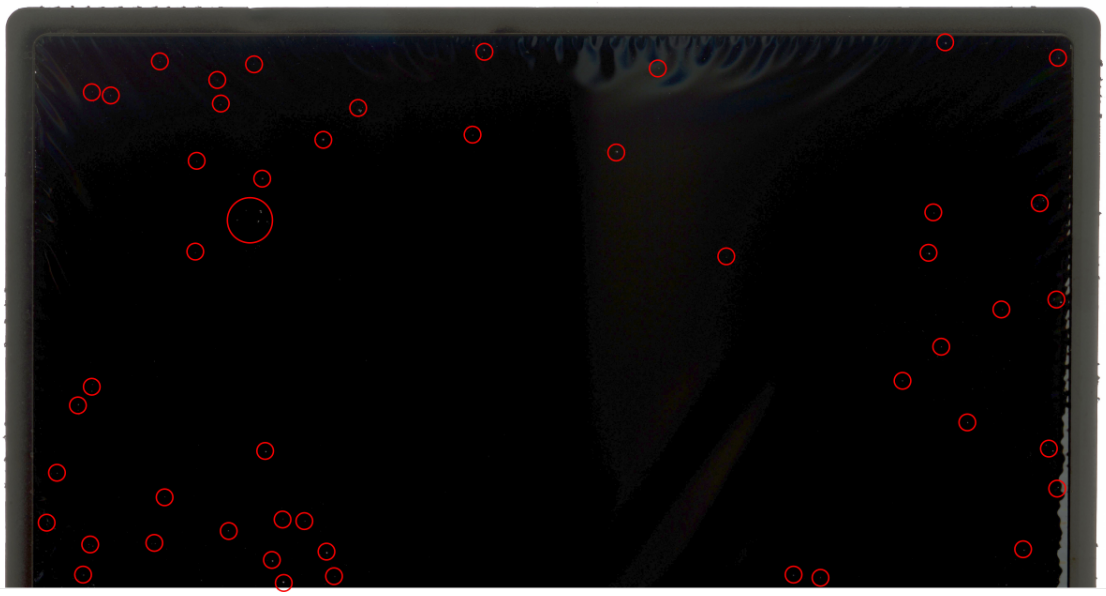

Figure 8. Portion of a filter prototype image acquired in transmission mode with a high resolution scanner. The membrane is 2 μm of PI and 200 nm of aluminum. Early prototypes such as this presented a high number of pinholes, highlighted in the picture by red circles.

3.3 Thermal cycling in vacuum

Temperature cycling test under vacuum is performed on the filters to verify that thermal stress does not affect the assembly integrity, causing a detachment between the components of the filter. Two different kind of samples were investigated: bare 2 um thick PI membrane and 2 um PI membrane coated with 200 nm of aluminum. Both types are mounted on 200 μm-thick nickel circular frames with aperture diameter of about 16 mm. In particular, we tested two bare PI samples and six PI/Al samples. All the samples described are small-scale early-stage prototypes manufactured by IHEP.

The tests were performed using a cryogenic test chamber set-up at INAF/OAPA. Such a setup is able to cycle through the chosen temperatures in a specific range with a defined ramp rate (a few K/min) and hold time, within a temperature range of 15–320 K. The experimental setup consists of a cylindrical vacuum chamber with 200 mm inner diameter, a vacuum pump system (turbo+scroll), a mechanical cooling system based on a He closed cycle, and a heater powered by a dedicated controller. Two thermometers are available, one measuring the temperature of the cooling system cold head, and the other measuring the sample holder plate temperature. A custom computer software, interfaced with the temperature controller, allows to set, start, and monitor the thermal cycling. The plate of the experimental chamber allowed mounting concurrently eight samples, as shown in Fig. 9.

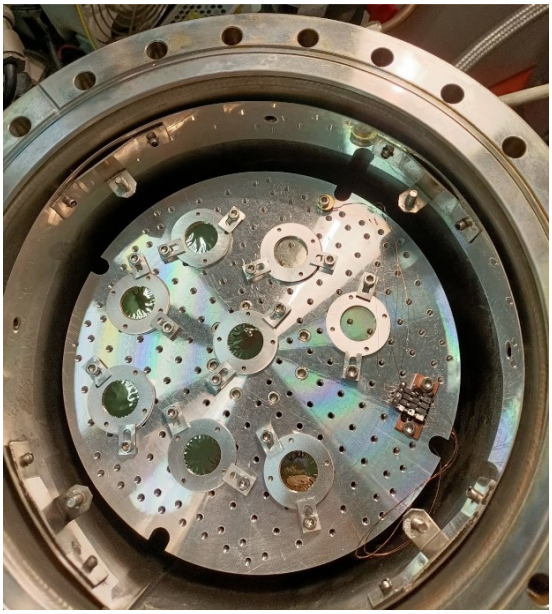

Figure 9. Photos of the mounting of the samples under test.

The samples were placed on the plate inside the chamber, the chamber closed with a viewport lid and vented, and finally the computer started the temperature cycle as programmed, while a sensor within the chamber measured the sample temperature. A camera was placed on top of the lid window, to acquire pictures of the sample at the beginning of each cycle segment. Tab. 2 summarizes the thermal cycle parameters used during the thermal cycle test.

Figure 10 shows a plot of the thermal cycles (25 cycles between Tmax and Tmin), where the stability of the single cycle, the T ramp slope and holding time can be checked.

The thermal cycles were correctly completed in approximately 78 hours. A visual inspection with a high resolution photographic scanner was performed before and after the thermal cycles, and no damages, detachments or alterations of the filter surfaces were observed.

An aluminum interface has been designed to accommodate full-scale LAD filters. The filters that will be produced by the industry are going to be subject to the thermal cycling test.

Table 2. Test parameters for thermal cycling.

Minimum Temperature	Tmin	190 K
maximum Temperature	Tmax	310 K
Temperature ramp	Tramp	2 K/min
Hold time	Ht	20 min
Number of cycles	N cycles	25
Pressure in the chamber	P	2.5e-5 mbar

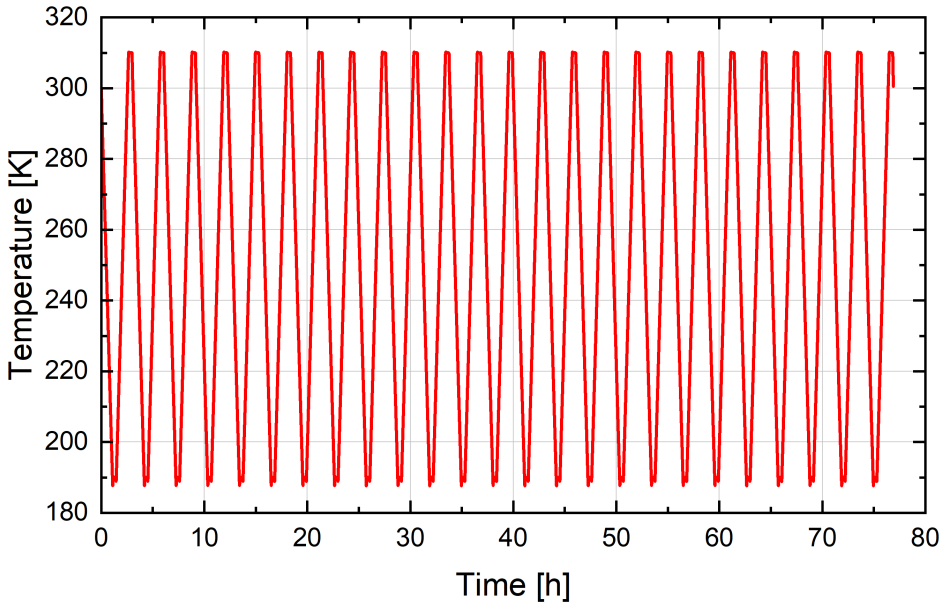

Figure 10. Complete thermal cycling test, showing the maximum and minimum temperatures reached, the temperature ramp and the holding time.

3.4 Static differential pressure bulge test

A bulge test system has been set-up in the INAF-OAPA laboratories to study the mechanical properties of thin suspended membranes such as the LAD filters. The study is performed by analyzing the membrane curvature, acquiring linear profiles, while applying a controlled differential pressure to it. The experimental setup comprises a XY-translator to move the filter along its plane, an optical distance sensor to measure the film deflection, a sample-holder and an electronically regulated pressuring system to apply and measure the differential pressure (see Fig. 14). The filter is mounted on a custom sample holder, sealed on the filter frame with an o-ring to allow the pressurization of the bottom face. The sample holder is attached to the computer controlled translator, which moves the bulged filter for measuring the membrane profiles with the sensor. A photo of the system is shown in Fig. 13. The pressuring system adopts a precise electronic pressure regulator (Equilibar model QPV), and a couple of pressure reducer valves (high and low-pressure stages) connected to a pressurized dry nitrogen tank. The pressuring system allows to compensate small gas leaks, regulating the pressure with an accuracy of 0.17 mbar. The scanning of the sample is performed along one of its axes while the differential pressure is kept constant for all the duration of the acquisition, and the maximum displacement (at the center of the filter) is extracted from the curve. The displacement measurement is performed by a Micro-epsilon optical confocal sensor, which allows high accuracy of the measurement, allowing for a good resolution along the filter plane thanks to the small beam spot diameter. Particular care was taken in setting the scan parameters such as scan speed, sample frequency, and peak selection to pursue a reliable profile measurement. The scan speed is a trade-off between the duration and the stability of the measure, a reasonable value was found to be 1.7 mm/s.

Two full-scale LAD filter prototypes, produced at IHEP laboratories, were tested with the differential pressure system. The first one, LAD#01, is made of a 2 μm thick PI membrane with 200 nm of Al coating, and was tested up to 10 mbar. The second, LAD#02, has the same thickness of polyimide, but a 300 nm thick Al coating, and was tested up to 15 mbar. Fig. 12 shows LAD#01 mounted on the sample holder during the tests.

In Fig. 11 the max bulge height acquired on the top of the domed film vs. the differential pressure value is reported for the LAD#01 and LAD#02 filters. At pressures approaching zero, an initial bulge height with value $>$ 1 mm was found on the LAD#01, indicating a slack membrane. Higher initial height value, thus more slackness, was measured on the LAD#02 membrane. Since the initial height value for the two filter under test are different a direct comparison on the maximum bulge height cannot be done, but, considering the maximum height minus the initial height, we obtain a a deformation about 25% higher for LAD#01. That is justified by the stiffening due to the extra amount of aluminum, and partly due to the higher initial height that produce a more pronounced dome shape.

The elastic properties of the composite membrane (biaxial and elastic modulus) composed by the plastic film and the aluminum coating could be retrieved by adopting a mixed experimental-numerical approach based on the analysis of the bulge test data.[21]

The results of the test was used to tune the LAD module design, to ensure enough space between the filter and the collimator. The flight filters will be produced by industry based on a process that presents some differences with respect to the process used to produce the first prototypes. They are expected to be flat, and lacking the slackness measured on the tested filters.

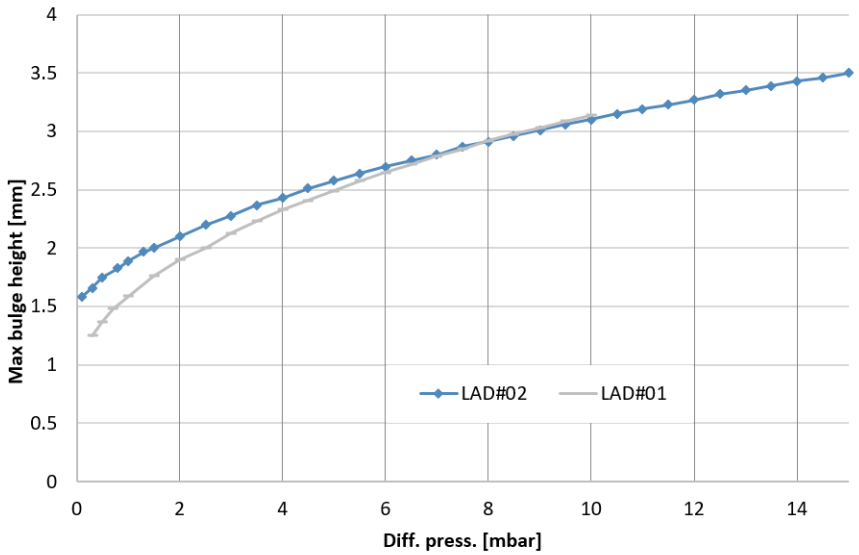

Figure 11. Measures of the maximum bulge height vs. differential pressure applied to the filters.

3.5 Set-up for bright Earth test

As described in sec. 2.6, attenuating the light originated by the bright Earth is one of the primary goals of the filters. Experimentally testing this capability, however, is challenging because of the very high attenuation provided, that falls much below the sensitivity of transmission spectrophotometers. Measurements at specific wavelengths can be performed using laser sources, that would provide a much stronger impinging flux and a measurable filtered one. With the goal of testing the filters throughout the spectral range of interest (300–1100 nm), and with a realistic spectrum, we have designed a test system based on a solar simulator used as radiation source. An ABET Technologies 11002 SunLite simulator, available at UNIPA, will be used for the preliminary testing, providing a $\sim$50$\times$50 mm 1 sun irradiated area using a 100 W Xe arc lamp. An AM0 filter mounted in the solar simulator allows to obtain a spectrum equivalent to the solar spectrum outside the

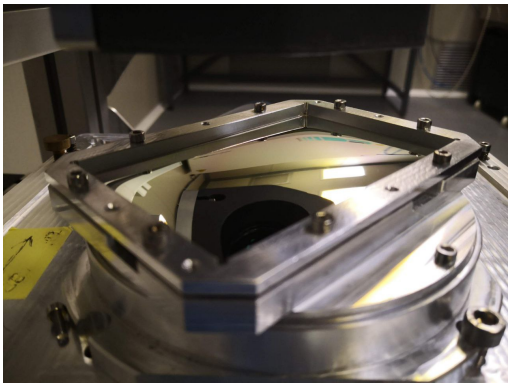

Figure 12. LAD#01 filter mounted in the bulge test holder during a measurement.

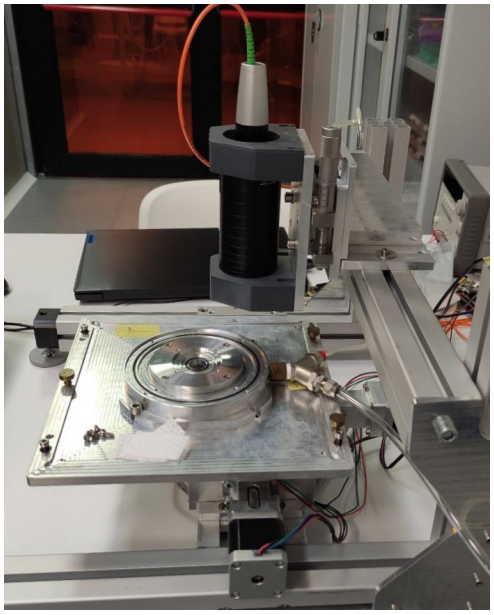

Figure 13. Photo of the bulge test setup.

Earth atmosphere. A light-tight box provide a mounting flange for the filter and a collimator tube enclosing the light flux measuring detector. Two different calibrated photodiodes are used to measure the flux with and without the filter under test interposed between the source and the detector. We selected a Hamamatsu S1336-5BK photodiode for the measurement of the reference unfiltered flux. The detector response range is 320–1100 nm, with a photosensitivity of 0.5 A/W at 960 nm, and an active area of 5.76 mm^2. The filtered

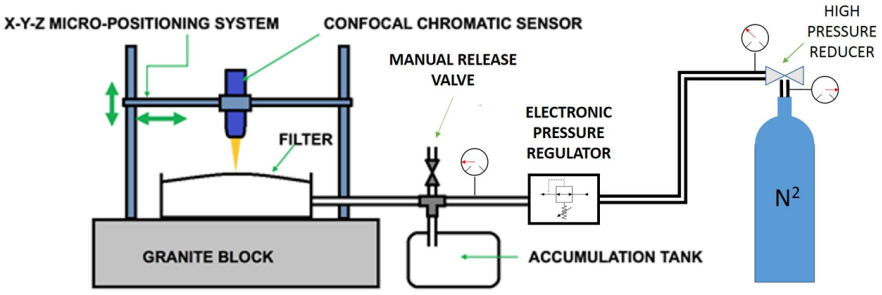

Figure 14. Schematic drawing of the bulge test setup.

flux, strongly attenuated, is expected to have a power, integrated over all the spectrum, of about 160 fW. In orded to measure such small flux with a calibrated detector, we selected a Hamamatsu S9295 photodiode, with on-board preamplification and thermo-electric cooling (working temperature -25 °C). It has a large active area of 10 mm^2 and a response range of 190–1100 nm, and provide a photosensitivity of 5.1 V/nW at 960 nm, and noise equivalent power of 4 $fW/Hz^{0.5}$ at 10 Hz. At the time of writing, the measurement setup is being assembled and tested at the INAF-OAPA laboratories.

3.6 Planned AO test campaign

The resistance of the LAD filters to atomic oxygen erosion is of primary importance as mentioned in sec. 2.1, and experimental characterization is needed to ascertain whether the filter polyimide is safe from the degradation involved. The two elements protecting the PI are the aluminum coating and the capillary plate collimator. The first constitutes a blocking layer, potentially capable of stopping the penetration of oxygen atoms; its protection effectiveness depends on the quality of the coating, since porosity or defects of the film would constitute entrance windows for the AO. The collimator is a 5 mm thick glass plate with parallel microchannels with 83 μm diameter and an open area ratio $> 50\%$. It would prevent any oxygen atom to directly reach the underlying filter with angles $> 0.95°$ with respect to the direction normal to the filter plane. If a collimator equipped instrument flies even with a slight deviation angle with respect to the spacecraft trajectory, it is possible that the AO erosion would have a very low rate, and eventually cease to be an issue. It is possible, nonetheless, that atoms impinging on the collimator could ricochet inside the pores and reach the filter with enough energy to break the PI molecules and cause erosion, as suggested from past studies regarding AO scattering phenomena.[22]

A test campaign is planned at ESTEC ATOX facility[23] to be performed on the first industry-manufactured filters as soon as they will be available. Multiple characterization techniques will be used to study the samples before and after the test campaign, for assessing the eventual erosion damage. Several sample configurations will be tested, including the baseline filter design and filters coupled with capillary plate collimators. Also, filters with an additional protective layer of Al_2O_3 deposited by atomic layer deposition over the Al will be tested.

4. CONCLUSIONS

The design of the LAD filters is a delicate trade-off between conflicting needs and requirements. The baseline filter composition has been selected with the aid of modeling and simulations, and the characterization tests performed so far (see also 3) indicate that it is able to meet the requirements. To fully demonstrate the filter technology, more characterization tests are in order, in particular concerning the resistance to AO and the IR/Vis/UV attenuation performance. Accordingly, we are assembling the proper measurement systems and have planned test campaigns.

ACKNOWLEDGMENTS

This research has received funding and support by the Italian Space Agency project “eXTP phase B2” (agreement 2020-3-HH.0 and addendum 2020-3-HH.1-2021).

REFERENCES

[1] Zhang, S. et al., “The enhanced x-ray timing and polarimetry mission - eXTP,” *Science China Physics, Mechanics and Astronomy* **62** (dec 2018).

[2] Feroci, M. et al., “The Large Area Detector onboard the eXTP mission,” in [*Space Telescopes and Instrumentation 2018: Ultraviolet to Gamma Ray*], den Herder, J.-W. A., Nikzad, S., and Nakazawa, K., eds., **10699**, 281 – 295, International Society for Optics and Photonics, SPIE (2018).

[3] Chen, T., Gao, N., Chen, Y., Xu, Y., Lu, F., Cao, J., Xu, X., Lo Cicero, U., Barbera, M., and Feroci, M., “Optical thermal filters for eXTP: manufacturing and characterization,” in [*Space Telescopes and Instrumentation 2020: Ultraviolet to Gamma Ray*], den Herder, J.-W. A., Nikzad, S., and Nakazawa, K., eds., **11444**, 1232 – 1243, International Society for Optics and Photonics, SPIE (2020).

[4] Zhang, S.-N. et al., “Overview to the hard x-ray modulation telescope (insight-HXMT) satellite,” *Science China Physics, Mechanics, and Astronomy* **63** (feb 2020).

[5] Garmire, G. P., Bautz, M. W., Ford, P. G., Nousek, J. A., and George R. Ricker, J., "Advanced CCD imaging spectrometer (ACIS) instrument on the chandra x-ray observatory," in [*X-Ray and Gamma-Ray Telescopes and Instruments for Astronomy*], Truemper, J. E. and Tananbaum, H. D., eds., SPIE (Mar. 2003).

[6] Barbera, M., Winter, B., Coker, J., Feroci, M., Kennedy, T., Walton, D., and Zane, S., "Baseline design of the filters for the LAD detector on board LOFT," in [*Space Telescopes and Instrumentation 2014: Ultraviolet to Gamma Ray*], Takahashi, T., den Herder, J.-W. A., and Bautz, M., eds., **9144**, 1876 – 1886, International Society for Optics and Photonics, SPIE (2014).

[7] Barbera, M., Lo Cicero, U., Sciortino, L., D'Anca, F., Lo Cicero, G., Parodi, G., Sciortino, S., Rauw, G., Branduardi-Raymont, G., Varisco, S., Bonura, S. F., Collura, A., Candia, R., Cicca, G. D., Giglio, P., Buttacavoli, A., Cuttaia, F., Villa, F., Cappi, M., Trong, T. L., Mesnager, J.-M., Peille, P., den Hartog, R., den Herder, J. W., Jackson, B., Barret, D., and Piro, L., "ATHENA X-IFU thermal filters development status toward the end of the instrument phase-A," in [*Space Telescopes and Instrumentation 2018: Ultraviolet to Gamma Ray*], den Herder, J.-W. A., Nikzad, S., and Nakazawa, K., eds., **10699**, 406 – 420, International Society for Optics and Photonics, SPIE (2018).

[8] Barbera, M., Lo Cicero, U., Sciortino, L., D'Anca, F., Parodi, G., Rataj, M., Polak, S., Pilch, A., Meidinger, N., Sciortino, S., Rauw, G., Raymont, G. B., Mineo, T., Perinati, E., Giglio, P., Collura, A., Varisco, S., and Candia, R., "ATHENA WFI optical blocking filters development status toward the end of the instrument phase-A," in [*Space Telescopes and Instrumentation 2018: Ultraviolet to Gamma Ray*], den Herder, J.-W. A., Nikzad, S., and Nakazawa, K., eds., **10699**, 373 – 385, International Society for Optics and Photonics, SPIE (2018).

[9] Banks, B. A., de Groh, K. K., and Miller, S. K., "Low earth orbital atomic oxygen interactions with spacecraft materials," *MRS Proceedings* **851** (2004).

[10] Heavens, O. S., "Optical properties of thin films," *Reports on Progress in Physics* **23**, 1–65 (Jan. 1960).

[11] Cavadi, A., Artale, M. A., Barbera, M., Collura, A., Powell, F. R., and Varisco, S., "Measurement of optical constants n and k of lexan and polyimide," in [*EUV, X-Ray, and Gamma-Ray Instrumentation for Astronomy X*], Siegmund, O. H. W. and Flanagan, K. A., eds., SPIE (Oct. 1999).

[12] Henke, B., Gullikson, E., and Davis, J., "X-ray interactions: Photoabsorption, scattering, transmission, and reflection at e = 50-30, 000 eV, z = 1-92," *Atomic Data and Nuclear Data Tables* **54**, 181–342 (July 1993).

[13] Palik, E. D., [*Handbook of optical constants of solids*], Academic press (1997).

[14] Hagemann, H.-J., Gudat, W., and Kunz, C., "Optical constants from the far infrared to the x-ray region: Mg, al, cu, ag, au, bi, c, and al2o3," *Journal of the Optical Society of America* **65**, 742–744 (jun 1975).

[15] Rakić, A. D., "Algorithm for the determination of intrinsic optical constants of metal films: application to aluminum," *Appl. Opt.* **34**, 4755–4767 (Aug 1995).

[16] Glenar, D. A., Stubbs, T. J., Schwieterman, E. W., Robinson, T. D., and Livengood, T. A., "Earthshine as an illumination source at the moon," *Icarus* **321**, 841–856 (2019).

[17] Stephens, G. L., O'Brien, D., Webster, P. J., Pilewski, P., Kato, S., and lin Li, J., "The albedo of earth," *Reviews of Geophysics* **53**, 141–163 (mar 2015).

[18] Krumrey, M. and Ulm, G., "High-accuracy detector calibration at the ptb four-crystal monochromator beamline," *Nuclear Instruments and Methods in Physics Research Section A: Accelerators, Spectrometers, Detectors and Associated Equipment* **467-468**, 1175–1178 (2001). Proceedings of the 7th Int. Conf. on Synchrotron Radiation Instru mentation.

[19] Nannarone, S., Borgatti, F., DeLuisa, A., Doyle, B. P., Gazzadi, G. C., Giglia, A., Finetti, P., Mahne, N., Pasquali, L., Pedio, M., Selvaggi, G., Naletto, G., Pelizzo, M. G., and Tondello, G., "The bear beamline at elettra," *AIP Conference Proceedings* **705**(1), 450–453 (2004).

[20] Barbera, M., Candia, R., Collura, A., Cicca, G. D., Pelliciari, C., Sciortino, S., and Varisco, S., "The palermo XACT facility: a new 35 m long soft x-ray beam-line for the development and calibration of next-generation x-ray observatories," in [*Proc. SPIE, Space Telescopes and Instrumentation II: Ultraviolet to Gamma Ray*], Turner, M. J. L. and Hasinger, G., eds., **6266**, SPIE (June 2006).

[21] Montinaro, N., Lo Cicero, U., D'Anca, F., Bozzo, E., Paltani, S., and Barbera, M., "Elastic characterization of nanometric plastic film for astrophysics application with an experimental-numerical method," *Thin Solid Films* **submitted** (2022).

[22] Banks, B. A., de Groh, K. K., Miller, S. K., Waters, D. L., and Kleiman, J. I., "Lessons learned from atomic oxygen interaction with spacecraft materials in low earth orbit," in [*AIP Conference Proceedings*], AIP (2009).
[23] Barbier, C., Flebus, C., and Van Eesbeek, M., "Atox - the estec atomic oxygen simulation facility," *Preparing for the Future* **2** (1992).